The Birth of a Type-II Nanostructure: Carrier Localization and Optical Properties of Isoelectronically Doped CdSe:Te Nanocrystals

Lijun Zhang,[†,*] Zhibin Lin,[†,‡,*] Jun-Wei Luo,[†] and Alberto Franceschetti[†,*]

[†]National Renewable Energy Laboratory, Golden, Colorado 80401, United States and [‡]Department of Physics, Colorado School of Mines, Golden, Colorado 80401, United States

ABSTRACT

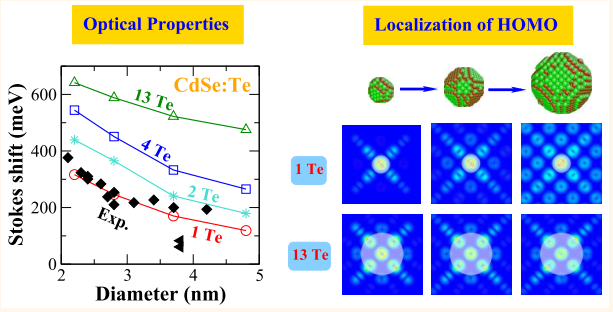

CdTe/CdSe core/shell nanocrystals are the prototypical example of type-II nanoheterostructures, in which the electron and the hole wave functions are localized in different parts of the nanostructure. As the thickness of the CdSe shell increases above a few monolayers, the spectroscopic properties of such nanocrystals change dramatically, reflecting the underlying type-I → type-II transition. For example, the exciton Stokes shift and radiative lifetime increase, while the decreasing biexciton binding energy changes sign from positive to negative. Recent experimental results for CdSe nanocrystals isoelectronically doped with a few Te substitutional impurities, however, have revealed a very different dependence of the optical and electronic properties on the nanocrystal size. Here we use atomistic calculations based on the pseudopotential method for single-particle excitations and the configuration–interaction approach for many-particle excitations to investigate carrier localization and electronic properties of CdTe/CdSe nanocrystals as the size of the CdTe core decreases from a few nm (characteristic of core/shell CdTe/CdSe nanocrystals) to the single impurity limit. We find that the unusual spectroscopic properties of isoelectronically doped CdSe:Te nanocrystals can be rationalized in terms of the change in the localization volume of the electron and hole wave functions as the size of the nanocrystal increases. The size dependence of the exciton Stokes shift, exciton radiative lifetime, and biexciton binding energy reflects the extent of carrier localization around the Te impurities.

KEYWORDS: type-II nanostructures · isoelectronically doped nanocrystals · electronic and optical property · exciton

The ability to grow nanostructures consisting of two or more semiconductors (nanoheterostructures) has dramatically increased the range of nanomaterials available for optoelectronic applications. Nanoheterostructures can be broadly classified in two categories: Type-I nanostructures, in which the electron and the hole wave functions (in their respective ground states) are localized in the same region of space within the nanostructure, and type-II nanostructures, in which the electron and the hole wave functions are localized in different regions of space—usually corresponding to different materials. Examples of type-II nanostructures include GaSb/GaAs[1] and Ge/Si[2] self-assembled quantum dots grown by molecular beam epitaxy, CdTe/CdSe,[3] CdTe/CdS,[4] CdSe/ZnTe,[3] CdS/ZnSe,[5] and CdS/CdTe[6] core/shell nanocrystals and nanorods grown by colloidal chemistry methods, as well as Ge/Si,[7] GaN/GaP,[8] and ZnO/ZnSe[9] coaxial core/shell quantum wires grown by vapor–liquid–solid or chemical vapor deposition. Type-II nanostructures encompass a wide range of physical properties that are not readily accessible in conventional type-I nanostructures: (i) type-II nanostructures typically emit light at lower energy than their individual constituents;[3] (ii) electron–hole spatial separation results in longer exciton radiative lifetimes;[1,10,11] (iii) interfacial exciton dissociation can occur even in the absence of a built-in electric field,[12,13] which may considerably simplify the architecture of nanostructure-based solar cells; (iv) strong electron–electron and hole–hole Coulomb repulsion leads to a blue shift of the biexciton absorption energy with respect to the single-exciton emission energy, which may enable lower gain thresholds in nanostructure lasers;[5] (v) reduced electron–hole overlap tends to decrease the Auger recombination rate of charged excitons and multiexcitons,[11] which may contribute to mitigate blinking effects in individual nanocrystals.[14]

While in planar, lattice matched heterostructures the spatial localization of the electron and hole wave functions is entirely

* Address correspondence to alberto.franceschetti@nrel.gov, lijun_physics@yahoo.com.cn.

Received for review July 9, 2012 and accepted August 19, 2012.

Published online August 19, 2012
10.1021/nn303060r

determined by the valence and conduction-band offsets between the constituents, carrier localization in a nanoheterostructure is also affected by nonhomogenous strain fields, quantum confinement effects, electron–hole Coulomb interactions, and correlation effects, which may alter the localization of the electron and hole wave functions[15] and therefore determine the type-I/type-II character of the nanostructure. Detailed experimental studies of CdTe/CdSe core/shell nanocrystals[3,10,16–22] have shown that such nanostructures undergo a type-I→type-II transition when the CdSe shell thickness exceeds a certain value, which depends on the size of the CdTe core. In the type-I regime, both the electron and the hole are localized primarily in the CdTe core. In the type-II regime, the hole is localized in the CdTe core, while the electron is localized in the CdSe shell. This type-I→type-II transition manifests itself with gradual but dramatic changes in the spectroscopic properties of CdTe/CdSe nanocrystals as the CdSe shell thickness increases. These changes include (i) a significant red shift of the emission energy, as the electron energy level approaches the CdSe band edge,[3,16–22] (ii) a broadening of the absorption peaks and the appearance of a low-energy absorption tail, due to the onset of spatially indirect absorption transitions,[10,18,19] (iii) an increase of the exciton radiative lifetime by a factor of 2 or more,[10,16,17,19,22] and (iv) a change of sign (from positive to negative) of the biexciton binding energy.[10,23]

The properties of spherical CdTe/CdSe core/shell nanocrystals can be mapped onto a D_c/D_s diagram, where D_c is the CdTe core radius and D_s is the CdSe shell thickness. Most experimental results for this system have been obtained in the regime of relatively large D_c (2–4 nm) and variable D_s.[3,17,18] Recently, it has become possible to dope CdSe nanocrystals with a few Te atoms, which, according to the experimental analysis of Franzl *et al.*,[24] leads to the formation of very small CdTe clusters embedded in the CdSe nanocrystals. This regime corresponds to the $D_c \to 0$ limit of the D_c/D_s diagram. The spectroscopic properties of such Te-doped CdSe nanocrystals were found to differ significantly from those of CdTe/CdSe core/shell nanocrystals, but the origin of those differences is not fully understood. Furthermore, the properties of CdTe/CdSe core/shell nanocrystals with small but finite core size ($0 < D_c < 2$ nm) are virtually unexplored. In this work, we are concerned with the evolution of the electronic structure of CdTe/CdSe nanocrystals as the size of the CdTe core decreases, all the way down to the single Te impurity limit.

Since the hole wave function of a CdTe cluster embedded in CdSe is strongly localized,[10] one may expect that the type-II character of a CdTe/CdSe core/shell nanocrystal would persist even in the impurity limit. However, recent experimental results for Te-doped CdSe nanocrystals have suggested a more subtle picture.[25,26] For instance, the exciton radiative lifetime of CdSe:Te nanocrystals (with 5% Te content in the injected solution) is quite large (50–70 ns), which is suggestive of a type-II character. However, the exciton lifetime was found to *decrease* as the size of the CdSe nanocrystal increases,[25] which is opposite to the trend found in type-II core/shell nanocrystals.[10,16,19,22] Similarly, the biexciton emission peak of Te-doped CdSe nanocrystals is blue-shifted with respect to the single-exciton emission peak by as much as 300 meV, which is indicative of enhanced electron–electron and hole–hole repulsion, suggesting a type-II band alignment.[5] However, the biexciton blue shift *decreases* as the diameter of the CdSe nanocrystal increases,[25] which again is in contrast with the behavior of core/shell nanocrystals.[10]

To address these apparently conflicting observations, we have performed atomistic quantum-mechanical calculations of the electronic and optical properties—including the exciton energy, lifetime, and fine structure, as well as the biexciton binding energy—for a series of Te-doped and core/shell CdSe nanocrystals of different size and composition. The calculations are based on the semiempirical pseudopotential method (SEPM) for the single-particle energy levels and wave functions,[27] and the configuration-interaction (CI) approach to calculate the excited-state energies and wave functions.[28] We found that the optical properties of Te-doped CdSe nanocrystals and CdTe/CdSe core/shell behave very differently as the size of the CdSe shell increases. This different size dependence can be rationalized in terms of the different behavior of the spatial localization of the CdTe-derived hole wave function. While in CdTe/CdSe core/shell nanocrystals the hole wave function is rather insensitive to the thickness of the CdSe shell, in Te-doped CdSe nanocrystals the localization of the hole wave function depends strongly on the size of the nanocrystal.

RESULTS AND DISCUSSION

Calculations of Optical Properties of Nanocrystals. Using the SEPM + CI method developed for large-scale atomistic calculations of semiconductor nanostructures (briefly described in the Method section), we calculated the following properties of CdTe/CdSe core–shell nanocrystals and Te-doped CdSe nanocrystals:

(i) *Exciton Stokes shift*, ΔE_X: The exciton Stokes shift is the energy difference between the first (linear) absorption peak and the lowest emission peak.[29] It is calculated here as $\Delta E_X = E_X^{max} - E_X^0$, where E_X^{max} is the energy of the exciton state that contributes the largest oscillator strength to the first absorption peak, and E_X^0 is the energy of the lowest exciton state (ground-state exciton). Both E_X^{max} and E_X^0 are calculated using our CI approach. In small-core CdTe/CdSe core/shell nanocrystals, E_X^{max} originates from spatially direct transitions

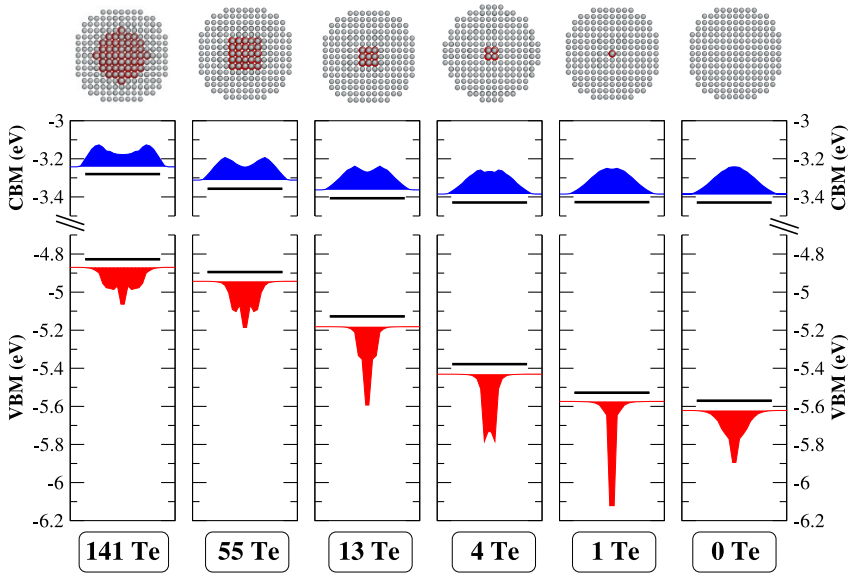

Figure 1. Quasi-particle energy and wave function amplitude of the band-edge states for a series of CdSe nanocrystals (D = 4.8 nm), as a function of the number of Te substitutional impurities. The upper panel shows the geometric arrangement of the Se (gray) and Te (red) atoms in the nanocrystals. The lower panel shows the energy level, and the spherically averaged wave function amplitude of the band-edge states, plotted along the radial direction of the nanocrystals.

in the CdSe region of the nanocrystal, while E_X^0 originates from spatially indirect transitions between the CdTe core and the CdSe shell. As a result, ΔE_X tends to increase as the type-II character becomes more pronounced.

(ii) *Exciton dark/bright splitting* ΔE_{DB}: It is well-known that in most semiconductor nanocrystals the lowest-energy exciton state is "dark" (optically forbidden). The exciton dark/bright splitting $\Delta E_{DB} = E_X^B - E_X^D$ is the energy difference between the first "bright" (optically allowed) state and the lowest-energy "dark" (optically forbidden) state. This splitting is caused by electron−hole exchange interactions.[28] ΔE_{DB} controls many spectroscopic properties of nanocrystals, such as the exciton lifetime and the photoluminescence intensity at the room temperature.

(iii) *Exciton radiative lifetime* τ_X: The exciton radiative lifetime is calculated as $1/\tau_X = \Sigma_i p_i(T)/\tau_i$, where $p_i(T)$ is the temperature-dependent occupation factor of exciton state i, and τ_i is its intrinsic lifetime. To determine $p_i(T)$, we use the Boltzmann distribution at temperature T based on the calculated CI energy levels for the exciton. The intrinsic lifetime τ_i is given by[30]

$$1/\tau_i = 4n_{out}F^2\alpha E_i^3|M|_i^2/3c^2 \quad (1)$$

where n_{out} is the refractive index of the surrounding medium (here we use n_{out} = 1.44, corresponding to the octadecene solvent used in experiments),[25] $F = 3\epsilon_{out}/(\epsilon_{nanocrystal} + 2\epsilon_{out})$ is the local field factor ($\epsilon_{out} = n_{out}^2$ and $\epsilon_{nanocrystal}$ is the effective dielectric constant of the nanocrystal), E_i and M_i are the energy and the CI dipole matrix element of the exciton state i, respectively, α is the fine structure constant, and c is the speed of light.

(iv) *Biexciton binding energy* Δ_{XX}: The biexciton binding energy is defined as $\Delta_{XX} = 2E_X^0 - E_{XX}^0$, where E_X^0 and E_{XX}^0 are the single-exciton and biexciton ground-state energies, respectively. It should not be confused with the "apparent" biexciton binding energy, which is obtained from the absorption or emission spectra of the biexciton.[29,31] In pure CdSe nanocrystals, the "apparent" binding energy is 10−20 meV larger than the "real" binding energy.[31] Positive values of Δ_{XX} indicate biexciton binding, which generally corresponds to a red-shift of the biexciton emission peak with respect to the single-exciton emission peak.[29] E_X^0 and E_{XX}^0 are calculated here using the CI approach.

Evolution from CdTe/CdSe Core/Shell Nanocrystals to Te-Doped CdSe Nanocrystals. Te-doped CdSe nanocrystals can be viewed as the limiting case of CdTe/CdSe core/shell nanocrystals when the size of the CdTe core is reduced. To illustrate the transition from a core/shell nanocrystal to a doped nanocrystal, we show in Figure 1 the electron and hole quasi-particle energies and wave functions of a series of CdTe/CdSe nanocrystals, in which the outer diameter is kept fixed at 4.8 nm, while the diameter of the CdTe core is decreased from 2.4 nm (corresponding to N_{Te} = 141) down to the single impurity limit (N_{Te} = 1). The nanocrystals are constructed in the zinc-blende lattice structure. Unless otherwise noted, the CdTe core (as well as the whole nanocrystal) has the T_d point-group symmetry, and is positioned at the center of the CdSe nanocrystal. For comparison, the electron and hole energies and wave functions of a 4.8 nm pure CdSe nanocrystal are also displayed in Figure 1. As the size of the CdTe core decreases, the hole wave function remains localized in the CdTe region, with modest spill

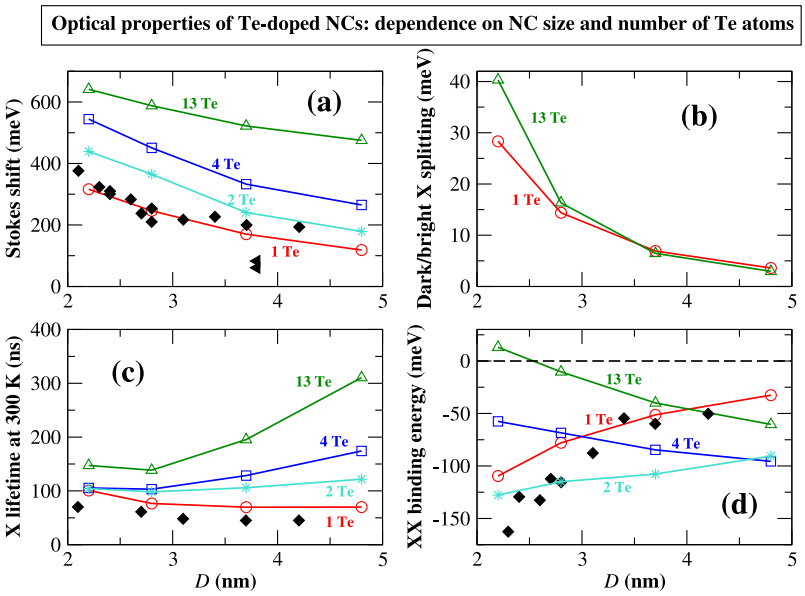

Figure 2. Evolution of the optical properties of Te-doped CdSe nanocrystals (NCs) as a function of the outer nanocrystal diameter: (a) exciton Stokes shift; (b) Energy splitting between the lowest-energy dark excitonic state and the first bright state; (c) exciton radiative lifetime at 300 K; (d) biexciton binding energy. Note that the Te_2 cluster has the C_2 (not T_d) point-group symmetry. Filled black symbols denote experimental results from ref 25 (diamonds) and ref 24 (left triangles).

over into the CdSe shell, even in the case of a single Te impurity. Because of increasing quantum confinement in the CdTe core, the hole energy decreases from −4.83 eV for the nanocrystal with a 141 Te atom core to −5.53 eV for the nanocrystal with a single Te impurity (the energies are referred to the vacuum level). The electron wave function, on the other hand, is delocalized over the entire nanocrystal. For larger CdTe cores ($N_{Te} \geq 13$) it has maximum amplitude on the CdSe shell, whereas for smaller CdTe cores ($N_{Te} < 13$) the relative amplitude of the electron wave function on the CdTe cluster increases. In the single Te impurity limit, the amplitude of the electron wave function at the center of the nanocrystal is almost unaffected by the presence of the Te atom. The electron energy increases as the size of the CdTe core increases, eventually approaching the conduction-band minimum energy of a CdTe nanocrystal of equivalent size. The wave function profiles shown in Figure 1 suggest that as the size of the CdTe core decreases, the exciton character is expected to change from type-II (hole localized in the CdTe core and electron localized primarily in the CdSe shell) to quasi-type-I (hole localized primarily in the CdTe core and electron extended over the whole nanocrystal region). In the following, we will discuss how electron and hole localization affects the optical properties of quasi-type-I Te-doped CdSe nanocrystals as a function of size.

Optical Properties of Te-doped CdSe Nanocrystals as a Function of Size. The spectroscopic properties of Te-doped CdSe nanocrystals were investigated in refs 25 and 26 and found to be different from those of CdTe/CdSe core/shell nanocrystals. In this section we correlate the size dependence of the optical properties of Te-doped CdSe nanocrystals with the energy and degree of localization of the band-edge states. Figure 2 shows the calculated single-exciton Stokes shift, dark/bright splitting, and radiative lifetime, as well as the biexciton binding energy, of a set of Te-doped CdSe nanocrystals, as a function of the nanocrystal outer diameter D. The exciton Stokes shift ΔE_X (Figure 2a) decreases monotonically as the size of the nanocrystal increases. This behavior is opposite to that observed in conventional CdTe/CdSe cores/shell nanocrystals (in which the CdTe core size typically exceeds 2 nm). In such core/shell nanocrystals, the exciton Stokes shift increases as the shell size increases and the type-I/type-II transition sets in.[10,18] The reason for the different behavior of Te-doped nanocrystals resides in the sensitive dependence of the hole energy levels on the nanocrystal size, which is shown in Figure 3a. While the ground-state exciton (of energy E_X^0) originates mainly from the (h_0, e_0) configuration, consisting of the Te-derived localized hole state h_0 (valence-band maximum) and the more delocalized electron state e_0 (conduction-band minimum), the first absorption peak (of energy E_X^{max}) originates primarily from configurations in which the electron state is still e_0, but the hole state is localized in the CdSe region of the nanocrystal (we denote such hole states as h_{CdSe}). The energy difference between h_0 and h_{CdSe} decreases as the size of the nanocrystal increases, as shown in Figure 3a. This shift is responsible for the decrease of the Stokes shift as D increases. Note that in the case of a single Te impurity ($N_{Te} = 1$), h_0 and h_{CdSe} converge to the same energy in the bulk limit (Figure 3a). This means that a

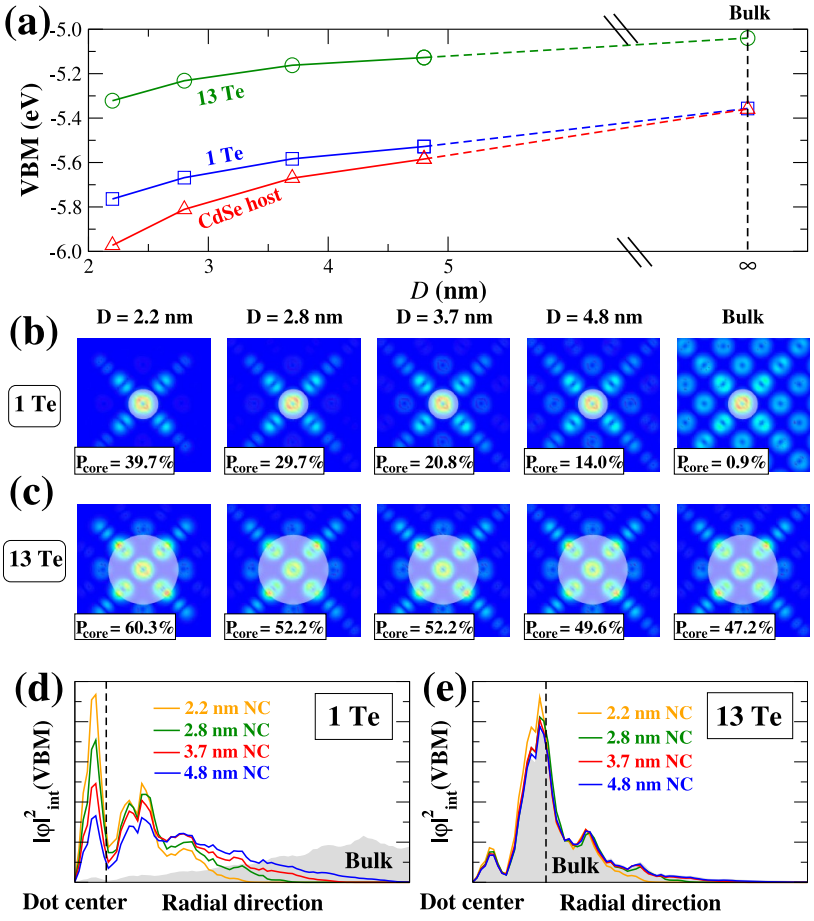

Figure 3. (a) Evolution of the valence-band maximum of CdSe nanocrystals containing 0, 1, and 13 Te impurities as the size of the nanocrystal is gradually increased up to the bulk limit. (b,c) Contour plots of the corresponding wave function amplitudes are shown in a plane cutting through the nanocrystal center, for the nanocrystal with D = 2.2, 2.8, 3.7, and 4.8 nm, as well as for bulk CdSe. The region corresponding to the small CdTe core is marked by a shaded circle. The integral of the wave function amplitude over the CdTe core region (P_{core}) is shown in each subplot as a percentage. The radius of the CdTe core is evaluated from the number of Te impurity atoms. (d,e) One-dimensional plots of the spherically averaged wave function amplitudes along the radial direction of the N_{Te} = 1 and N_{Te} = 13 doped nanocrystals, for different nanocrystal sizes.

single Te impurity in bulk CdSe forms a resonant hole state inside the valence band, and only introduces a slight modification of the hole wave function of the CdSe host. This result is also borne out of wave function amplitude plots, shown in Figure 3b,d, and is consistent with experimental probes of Te impurities in $CdS_{1-x}Se_x$ crystals[32] and ZnSe crystals.[33−35]

The size dependence of the dark/bright splitting ΔE_{DB} of two Te-doped nanocrystals (N_{Te} = 1 and N_{Te} = 13) is shown in Figure 2b. We see that ΔE_{DB} decreases rapidly as the nanocrystal size increases, as a result of the decreased electron−hole overlap, which is mainly due to a more spread out electron wave function. ΔE_{DB} drops more rapidly for N_{Te} = 13 than for N_{Te} = 1, reflecting the transition from the type-II regime (corresponding to charge separation) to the quasi type-I regime (corresponding to increased electron−hole overlap), as demonstrated in Figure 1.

Figure 2 panels c and d show the exciton lifetime and the biexciton binding energy of Te-doped nanocrystals as a function of nanocrystal size. Interestingly, we find that the N_{Te} = 1 doped nanocrystals, and to some extent also the N_{Te} = 2 doped nanocrystals, follow a different trend with size compared to nanocrystals with a larger CdTe core. The exciton lifetime τ_X (Figure 2c) of the N_{Te} = 1 doped nanocrystal decreases with increasing size, while the lifetime of the N_{Te} = 4 and N_{Te} = 13 nanocrystals increases with increasing size (except for very small nanocrystals, where the larger ΔE_{DB} (Figure 2b) leads to a significantly decreased population of the bright exciton states resulting in an increased lifetime). Equally remarkable is the fact that the magnitude of the negative biexciton binding energy Δ_{XX} (Figure 2d) decreases as a function of D for N_{Te} = 1, 2, whereas it increases as a function of D for $N_{Te} \geq 4$. This result can be explained by the fact that in the case N_{Te} = 1 the hole−hole Coulomb energy $J_{h,h}$ decreases very rapidly as the nanocrystal size D increases, as shown in Figure 4. In the case of larger CdTe cores ($N_{Te} \geq 4$), $J_{h,h}$ also decreases with increasing nanocrystal size, but at a much lower rate (Figure 4). Generally, the Coulomb interaction between the same

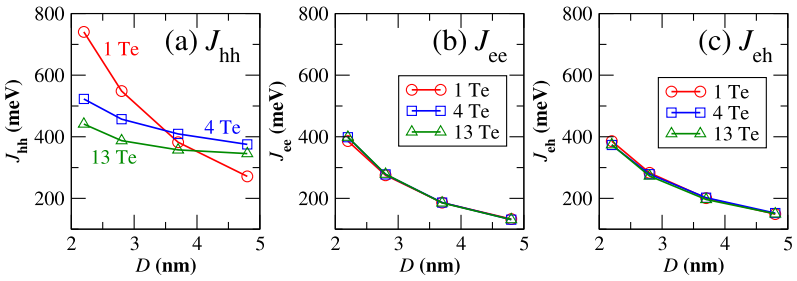

Figure 4. The calculated hole−hole (J_{hh}), electron−electron (J_{ee}), and electron−hole (J_{eh}) Coulomb integrals for the band-edge states of Te-doped CdSe nanocrystals (N_{Te} = 1, 4, 13) are shown as a function of the nanocrystal diameter *D*.

carriers is closely related to the carrier localization, *i.e.*, the stronger localization is favorable to larger Coulomb energy. The different size dependence of $J_{h,h}$ for different CdTe core sizes is a direct consequence of the different degree of hole localization, as illustrated in Figure 3b−e. For N_{Te} = 13 (Figure 3c,e) the hole wave function is strongly localized in the CdTe core for any size of the nanocrystal (including the case in the bulk limit). The projection of the hole wave function amplitude on the CdTe core region changes gradually from 60.3% for D = 2.2 nm, to 49.6% for D = 4.8 nm, to 47.2% in the bulk limit (Figure 3c), exhibiting weak size dependence. On the other hand, in the case of N_{Te} = 1 (Figure 3b,d), the degree of localization for the hole wave function is strongly size dependent. The projection on the CdTe core decreases dramatically from 39.7% for D = 2.2 nm to 14.0% for D = 4.8 nm, down to 0.9% in the bulk limit (Figure 3b). From this analysis, we conclude that the different behavior of Δ_{XX} as a function of D for small (N_{Te} = 1−2) *vs* large ($N_{Te} \geq 4$) CdTe cores is due to the different degree of hole localization in the CdTe core region.

Comparison between Theoretical Results and Experimental Data. Figure 2 shows available experimental data for the Stokes shift, the exciton lifetime, and the biexciton binding energy of Te-doped CdSe nanocrystals (to the best of our knowledge no experimental measurements of the dark/bright splitting in such nanocrystals are available). Experimental investigations of the spectroscopic properties of Te-doped CdSe nanocrystals are clouded by the fact that the number and location of the Te impurities in the nanocrystals is unknown, and also by the fact that such measurements are typically performed on ensembles of nanocrystals, so they are affected by inhomogenous broadening caused by the distribution of impurities within the nanocrystals, as well as the size and shape distribution of the nanocrystals. In the case of the exciton Stokes shift (Figure 2a), we find excellent agreement between our calculations for N_{Te} = 1−2 and the experimental results of ref 25. The calculated exciton radiative lifetime for N_{Te} = 1 (Figure 2c) is in reasonable agreement with the measured data.[25] Furthermore, the trend of calculated τ_X with nanocrystal size for N_{Te} = 1 (and to some extent also N_{Te} = 2) is consistent with that of experiment. In Figure 2d we compare the calculated biexciton binding energy Δ_{XX} with the measured "apparent" biexciton binding energy obtained from transient emission spectroscopy.[25] Our calculations for N_{Te} = 1 and N_{Te} = 2 are in good agreement with experiment, and have the same trend with size as the experimentally measured binding energy.

Effects of Geometry, Profile, and Location of Te Impurities. The comparison between our atomistic calculations and experimental results (Figure 2) strongly suggests that the spectroscopic features of the synthesized Te-doped CdSe nanocrystals are attributable to isolated, single Te substitutional impurities, or to clusters of at most two Te impurities. This does not necessarily imply, however, that each Te-doped nanocrystal will contain exactly one Te impurity or one pair of Te impurities. Because of strong wave function localization, the presence of multiple Te impurities in the same nanocrystal may have only modest effects on its spectroscopic properties, as long as the Te atoms are sufficiently apart from each other. To investigate this possibility, we considered a set of CdSe nanocrystals containing four spatially separated Te impurities, such that the smallest distance between any two Te atoms is larger than the cubic lattice constant. The positions of the Te impurities were kept fixed while the nanocrystal size was increased. The properties of such nanocrystals were then compared with those of nanocrystals containing a four-atom Te cluster at the center (N_{Te} = 4), and of nanocrystals containing a single Te atom at the center (N_{Te} = 1). We found that the exciton Stokes shift of the nanocrystal with four spatially separated Te impurities falls in between those of the N_{Te} = 4 nanocrystal and the N_{Te} = 1 nanocrystal (Figure 5a), and that the exciton lifetime for four separated Te impurities almost coincides with that of the N_{Te} = 1 nanocrystal (Figure 5b). These results suggest that, in the case of a single exciton, the nanocrystals with multiple, spatially separated Te impurities behave essentially in the same way as the nanocrystals with a single Te impurity.

In the case of the biexciton binding energy Δ_{XX}, however, we found that the value for four separated Te impurities is significantly smaller in magnitude than that for a single Te impurity, and that this discrepancy becomes larger as the nanocrystal size decreases, as

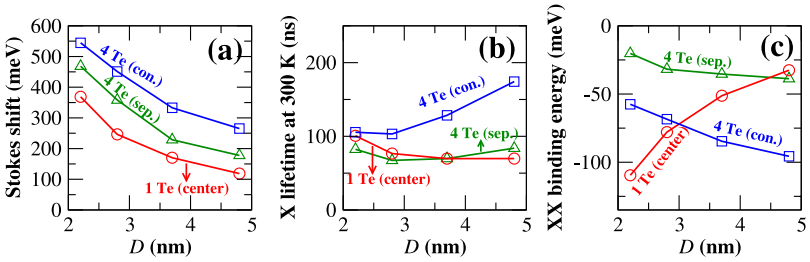

Figure 5. Comparison of the optical properties of Te-doped CdSe nanocrystals for different configurations of the Te substitutional impurities: Four spatially separated Te atoms (4Te-sep, see text for a more detailed description), a cluster of four Te atoms at the center of the nanocrystal (4Te-con), and a single Te atom at the center of the nanocrystal (1Te-center): (a) exciton Stokes shift; (b) radiative lifetime at 300 K; (c) biexciton binding energy.

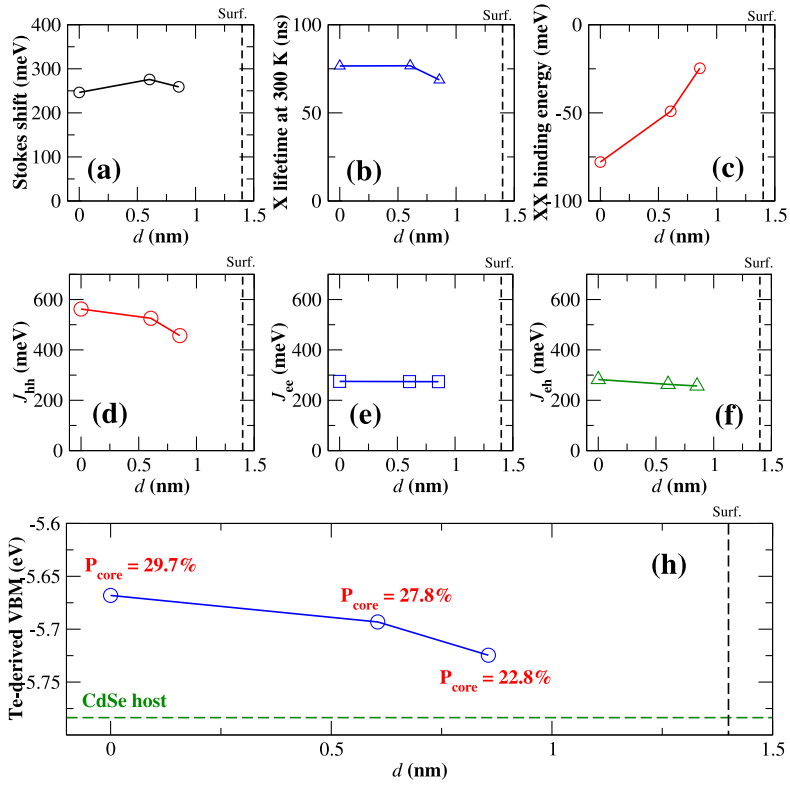

Figure 6. (Upper panels) Optical properties of a 2.8 nm CdSe nanocrystal doped with a single Te substitutional impurity, as the function of its distance (*d*) from the nanocrystal center: (a) exciton Stokes shift; (b) radiative lifetime at 300 K; (c) biexciton binding energy. (Middle panels) (d,e,f) The calculated hole−hole (J_{hh}), electron−electron (J_{ee}), and electron−hole (J_{eh}) Coulomb integrals for the band-edge states of such nanocrystals are shown as a function of *d*. (Lower panels) (h) The energy level of the (Te-derived) valence-band maximum of such nanocrystals is shown as a function of *d*. The energy of the CdSe-derived host state is shown for comparison (green horizontal dashed line). The integral of the wave function amplitude over the Te impurity region (P_{core}) is marked next to the individual data points. For all the subplots, the position corresponding to the nanocrystal surface (Surf.) is marked by a vertical dash line.

shown in Figure 5c. In fact, we find that the biexciton binding energy depends sensitively on the spatial location of the Te impurities. On the one hand, hole−hole Coulomb repulsion is expected to dissociate the biexciton into two excitons localized around two different Te impurities, and thus to reduce the magnitude of the (negative) biexciton binding energy. On the other hand, the quasi-particle energy splitting between hole states localized on separate Te impurities has the opposite effect of favoring localization of the biexciton around the Te impurity with the highest hole energy, thereby increasing the magnitude of the biexciton binding energy. The net effect will depend on the number and location of the Te impurities within the nanocrystal. For example, in the specific case of a 2.8 nm nanocrystal with four spatially separated Te impurities, we find that, in the single-configuration approximation, the ground-state biexciton configuration consists of two holes/excitons residing on the same Te atom (the one closest to the nanocrystal center), and the lowest-energy configuration with two holes/excitons located on different Te atoms is approximately 35 meV higher in energy. In the full CI calculation the ground-state biexciton exhibits

substantial mixing between those two configurations. This mixing is found to be enhanced by increased quantum confinement with decreasing nanocrystal size. Interestingly, such mixing of spatially separated excitons to form biexciton states has been reported in the CdSe nanocrystals, where the mixed phase biexciton, consisting of a nanocrystal exciton and a surface-trapped exciton, was found to exhibit the lower magnitude of the biexciton binding energy.[36−38]

To further illustrate the effect of the location of an isolated Te impurity on the optical properties of isoelectronically doped CdSe nanocrystals, the upper panels of Figure 6 show the exciton Stokes shift, radiative lifetime, and biexciton binding energy of a 2.8 nm CdSe nanocrystal with $N_{Te} = 1$, as a function of the distance d of the Te impurity from the center of the nanocrystal. As one can see, the exciton Stokes shift (Figure 6a) and exciton lifetime (Figure 6b) depend weakly on the location of the impurity across the nanocrystal. However, the (negative) biexciton binding energy (Figure 6c) decreases in magnitude from 75 meV for $d = 0$ nm to 25 meV for $d = 0.9$ nm. This substantial change of the biexciton binding energy originates from the sensitive dependence of the hole wave function localization on the location of the Te impurity. Figure 6h shows the corresponding energy level and integral of the wave function amplitude over the Te impurity region (P_{core}). A Te impurity near the nanocrystal surface leads to a shallower hole energy level (approaching the energy level of the CdSe host), and thus to a more delocalized hole wave function (smaller magnitude of P_{core}). While this has negligible effects on the Coulomb interaction between two electrons or between an electron and a hole, it results in significantly reduced Coulomb interaction between holes when the Te impurity approaches the nanocrystal surface (Figure 6d−f), thus reducing the magnitude of the (negative) biexciton binding energy (Figure 6c). For smaller nanocrystals containing spatially separated Te impurities, the Te impurities are located closer to the nanocrystal surface. This partially explains why in Figure 5c the magnitude of biexciton binding energy for four separated Te impurities decreases with decreasing diameters, and deviates remarkably from that of a single Te impurity at the center.

CONCLUSIONS

In summary, we have reported atomistic calculations of the electronic and optical properties of isoelectronically doped CdSe:Te nanocrystals. The calculations were performed using the empirical pseudopotential method to describe single-particle excitations, and the configuration−interaction approach to describe multiparticle excitations. The calculations reveal the changes in the localization of the electron and hole wave functions as the size of the CdTe core decreases from a few nm (typical of core/shell nanocrystals) to the single-impurity limit. The localization of the wave functions in turn determines the spectroscopic properties of such nanocrystals, and their dependence on the nanocrystal size. Our results clarify why the size dependence of the exciton Stokes shift, radiative lifetime, and the biexciton binding energy is different in isoelectronically doped CdSe:Te nanocrystals compared to core/shell CdTe/CdSe nanocrystals, as recently observed experimentally.

METHODS

The calculations of the electron and hole quasi-particle states were performed using the semiempirical pseudopotential method (SEPM), described in detail in refs 27 and 28. In this approach, the quasi-particle energies ϵ_i and wave functions ψ_i are obtained by solving the semiempirical single-particle Schrodinger equation:

$$\left[-\frac{\hbar^2}{2m}\nabla^2 + V_{loc}(\mathbf{r}) + \hat{V}_{SO}\right]\psi_i(\mathbf{r}) = \varepsilon_i\psi_i(\mathbf{r}) \qquad (2)$$

where $\hat{V}_{SO}$ is the nonlocal spin−orbit operator, and $V_{loc}(\mathbf{r})$ is the local potential, which is given by the superposition of screened atomic pseudopotentials centered at the atomic positions $\{\mathbf{R}_n\}$: $V_{loc}(\mathbf{r}) = \Sigma_n v_n(|\mathbf{r} - \mathbf{R}_n|)$. The Cd, Se, and Te atomic pseudopotentials are fitted to accurately reproduce the transition energies, effective masses, spin−orbit couplings, and deformation potentials of bulk CdSe and CdTe, as well as interface band offsets and alloy bowing parameters for the combined CdSe/CdTe system, as determined by ab initio calculations.[39] The nanocrystal surface is passivated using ligand-like pseudopotentials designed to remove surface states from the band gap.[27] Equation 1 is solved by expanding the wave functions in a plane-wave basis set with an energy cutoff of 6.88 Ryd. The band-edge states are calculated using the folded-spectrum method described in ref 40, which has a computational cost that scales only linearly with the size of the system. Because CdSe and CdTe have different bulk lattice constants (6.05 Å and 6.48 Å, respectively), CdTe/CdSe nanostructures are subject to a nonhomogeneous strain field, which is described here using the valence force field (VFF) method of Keating.[41,42] The minimization of the strain energy according to the VFF model yields the equilibrium positions $\{\mathbf{R}_n\}$ of the atoms in the nanostructure, which are then used to determine the local potential of eq 1.

Carrier−carrier interactions are included using the configuration−interaction (CI) method described in refs 28, 43, and 44. In this approach, the excited states are expanded in terms of Slater determinants obtained by promoting one electron (in the case of the single exciton) or two electrons (in the case of the biexciton) from the valence bands to the conduction bands. Coupling between Slater determinants is introduced by screened Coulomb and exchange interactions between carriers. To evaluate the Coulomb and exchange integrals, we use a phenomenological screening function that is position-dependent and size-dependent:[45]

$$\epsilon^{-1}(\mathbf{r}_1, \mathbf{r}_2) = \epsilon_{out}^{-1}(\mathbf{r}_1, \mathbf{r}_2) + [\epsilon_{in}^{-1}(\mathbf{r}_1, \mathbf{r}_2) - \epsilon_{out}^{-1}(\mathbf{r}_1, \mathbf{r}_2)]\, m(\mathbf{r}_1)\, m(\mathbf{r}_2) \qquad (3)$$

Here ϵ_{in} represents the dielectric function inside the nanocrystal, which is evaluated using the parameters of bulk CdSe following the Thomas−Fermi model proposed by Resta,[28,46] and ϵ_{out} is the dielectric constant of the surrounding medium

TABLE 1. Comparison of Calculated Exciton (E_X) and Biexciton (E_{XX}) Ground-State Energies Using Different Approaches[a]

	E_X (eV)			$E_{XX}/2$ (eV)		
	PT	SCF	CI	PT	SCF	CI
$Cd_{216}Se_{213}$	2.334	2.328	2.322	2.345	2.339	2.320
$Cd_{216}Se_{212}Te$	2.206	2.196	2.195	2.296	2.258	2.238
$Cd_{1000}Se_{1031}$	1.976	1.972	1.967	1.984	1.979	1.962
$Cd_{1000}Se_{890}Te_{141}$	1.404	1.403	1.392	1.422	1.419	1.385

[a] (i) First-order perturbation theory (PT), according to which $E_X = \varepsilon_e - \varepsilon_h - J_{e,h}$, and $E_{XX} = 2(\varepsilon_e - \varepsilon_h) - 4J_{e,h} + J_{h,h} + J_{e,e}$, where ε_e and ε_h are the quasi-particle energy of the electron and hole states, respectively, and $J_{i,j}$ are the screened Coulomb integrals. (ii) Self-consistent Hartree-like calculations (SCF). (iii) Configuration-interaction calculations (CI), using an active space for the basis sets consisting of 20 valence states and 10 conduction states. For this test, the screened Coulomb and exchange integrals are evaluated using a dielectric constant of 6.0.

(ϵ_{out} = 1 for vacuum is used here). Note that the dielectric constant of vacuum is used only to evaluate the Coulomb and exchange integrals, whereas for the radiative lifetime calculations, to directly compare with experimental data, we use the refractive index n_{out} = 1.44 (ϵ_{out} = 2.07), corresponding to the octadecene solvent used in experiments.[25] The mask function $m(\mathbf{r})$ is 1 for $|\mathbf{r} - \mathbf{r}_0| \leq R - d$ (where $\mathbf{r}_0$ is the center of the nanocrystal, R is its radius, and the transition layer $2d$ equals the CdSe bulk bond length), decays smoothly to zero as $[\sin(\pi(R - |\mathbf{r} - \mathbf{r}_0|)/2d) + 1]/2$ between $R - d$ and $R + d$, and vanishes for $|\mathbf{r} - \mathbf{r}_0| \geq R + d$.

The CI basis set is constructed from an active space consisting of 50 valence and 20 conduction states for the single exciton (corresponding to 4000 configurations), and 30 valence and 10 conduction states for the biexciton (corresponding to 336 300 configurations). The CI Hamiltonian $\hat{H}_{CI}$[28] is diagonalized in this basis set to yield the excited-state energies and wave functions of the nanostructure:

$$\hat{H}_{CI}\Psi^{(\alpha)} = E^{(\alpha)}\Psi^{(\alpha)} \quad (4)$$

We also performed self-consistent Hartree-like calculations[43] for the exciton and biexciton ground-state energies in some CdSe, Te-doped CdSe, and CdTe/CdSe core−shell nanocrystals, as shown in Table 1. We found that for all the cases considered here, the exciton and biexciton ground-state energies obtained from the self-consistent calculation are higher than those obtained from the CI calculation, suggesting that correlation effects, which are neglected in the Hartree-like calculation, are at least as important as the self-consistent effects, which are fully included in the Hartree-like calculation but only partially accounted for in the CI expansion.[31] In the present work, we therefore use the CI approach described above to calculate excitonic and multiexcitonic states.

Conflict of Interest: The authors declare no competing financial interest.

Acknowledgment. The authors acknowledge useful discussions with D. Oron. This work was supported by the US Department of Energy, Office of Science, Basic Energy Sciences, under Contract No. DE-AC36-08GO28308 to NREL. Z.L. is supported by the Renewable Energy Materials Research Science and Engineering Center (NSF Grant No. DMR-0820518) at the Colorado School of Mines and the National Renewable Energy Laboratory.

REFERENCES AND NOTES

1. Hatami, F.; Grundmann, M.; Ledentsov, N. N.; Heinrichsdorff, F.; Heitz, R.; Böhrer, J.; Bimberg, D.; Ruvimov, S. S.; Werner, P.; Ustinov, V. M.; *et al.* Carrier Dynamics in Type-II GaSb/GaAs Quantum Dots. *Phys. Rev. B* **1998**, *57*, 4635–4641.
2. Abstreiter, G.; Schittenhelm, P.; Engel, C.; Silveira, E.; Zrenner, A.; Meertens, D.; Jäger, W. Growth and Characterization of Self-Assembled Ge-Rich Islands on Si. *Semicond. Sci. Technol.* **1996**, *11*, 1521–1528.
3. Kim, S.; Fisher, B.; Eisler, H.-J.; Bawendi, M. Type-II Quantum Dots: CdTe/CdSe(Core/Shell) and CdSe/ZnTe(Core/Shell) Heterostructures. *J. Am. Chem. Soc.* **2003**, *125*, 11466–11467.
4. Dorfs, D.; Franzl, T.; Osovsky, R.; Brumer, M.; Lifshitz, E.; Klar, T. A.; Eychmüller, A. Type-I and Type-II Nanoscale Heterostructures Based on CdTe Nanocrystals: A Comparative Study. *Small* **2008**, *4*, 1148–1152.
5. Klimov, V. I.; Ivanov, S. A.; Nanda, J.; Achermann, M.; Bezel, I.; McGuire, J. A.; Piryatinski, A. Single-Exciton Optical Gain in Semiconductor Nanocrystals. *Nature* **2007**, *447*, 441–446.
6. Nonoguchi, Y.; Nakashima, T.; Kawai, T. Tuning Band Offsets of Core/Shell CdS/CdTe Nanocrystals. *Small* **2009**, *5*, 2403–2406.
7. Lauhon, L. J.; Gudiksen, M. S.; Wang, D.; Lieber, C. M. Epitaxial Core-Shell and Core-Multishell Nanowire Heterostructures. *Nature* **2002**, *420*, 57–61.
8. Lin, H.-M.; Chen, Y.-L.; Yang, J.; Liu, Y.-C.; Yin, K.-M.; Kai, J.-J.; Chen, F.-R.; Chen, L.-C.; Chen, Y.-F.; Chen, C.-C. Synthesis and Characterization of Core−Shell GaP@GaN and GaN@GaP Nanowires. *Nano Lett.* **2003**, *3*, 537–541.
9. Wang, K.; Chen, J.; Zhou, W.; Zhang, Y.; Yan, Y.; Pern, J.; Mascarenhas, A. Direct Growth of Highly Mismatched Type II ZnO/ZnSe Core/Shell Nanowire Arrays on Transparent Conducting Oxide Substrates for Solar Cell Applications. *Adv. Mater.* **2008**, *20*, 3248–3253.
10. Oron, D.; Kazes, M.; Banin, U. Multiexcitons in Type-II Colloidal Semiconductor Quantum Dots. *Phys. Rev. B* **2007**, *75*, 035330.
11. Ivanov, S. A.; Achermann, M. Spectral and Dynamic Properties of Excitons and Biexcitons in Type-II Semiconductor Nanocrystals. *ACS Nano* **2010**, *4*, 5994–6000.
12. Gross, D.; Mora-Sero, I.; Dittrich, T.; Belaidi, A.; Mauser, C.; Houtepen, A. J.; Como, E. D.; Rogach, A. L.; Feldmann, J. Charge Separation in Type II Tunneling Multilayered Structures of CdTe and CdSe Nanocrystals Directly Proven by Surface Photovoltage Spectroscopy. *J. Am. Chem. Soc.* **2010**, *132*, 5981–5983.
13. Zhu, H.; Song, N.; Lian, T. Wave-Function Engineering for Ultrafast Charge Separation and Slow Charge Recombination in Type II Core/Shell Quantum Dots. *J. Am. Chem. Soc.* **2011**, *133*, 8762–8771.
14. Osovsky, R.; Cheskis, D.; Kloper, V.; Sashchiuk, A.; Kroner, M.; Lifshitz, E. Continuous-Wave Pumping of Multiexciton Bands in the Photoluminescence Spectrum of a Single CdTe−CdSe Core−Shell Colloidal Quantum Dot. *Phys. Rev. Lett.* **2009**, *102*, 197401.
15. Franceschetti, A.; Wang, L. W.; Bester, G.; Zunger, A. Confinement-Induced *versus* Correlation-Induced Electron Localization and Wave-Function Entanglement in Semiconductor Nano Dumbbells. *Nano Lett.* **2006**, *6*, 1069–1074.
16. Jack, Li, J.; Tsay, J. M.; Michalet, X.; Weiss, S. Wavefunction Engineering: From Quantum Wells to Near-Infrared Type-II Colloidal Quantum Dots Synthesized by Layer-by-Layer Colloidal Epitaxy. *Chem. Phys.* **2005**, *318*, 82–90.
17. Chin, P. T. K.; Mello Donegá, C.; de; Bavel, S. S.; van; Meskers, S. C. J.; Sommerdijk, N. A. J. M.; Janssen, R. A. J. Highly Luminescent CdTe/CdSe Colloidal Heteronanocrystals with Temperature-Dependent Emission Color. *J. Am. Chem. Soc.* **2007**, *129*, 14880–14886.
18. de Mello Donegá, C. Formation of Nanoscale Spatially Indirect Excitons: Evolution of the type-II Optical Character of CdTe/CdSe Heteronanocrystals. *Phys. Rev. B* **2010**, *81*, 165303.
19. He, J.; Zhong, H.; Scholes, G. D. Electron-Hole Overlap Dictates the Hole Spin Relaxation Rate in Nanocrystal Heterostructures. *Phys. Rev. Lett.* **2010**, *105*, 046601.
20. Zhang, W.; Chen, G.; Wang, J.; Ye, B.-C.; Zhong, X. Design and Synthesis of Highly Luminescent Near-Infrared-Emitting Water-Soluble CdTe/CdSe/ZnS Core/Shell/Shell Quantum Dots. *Inorg. Chem.* **2009**, *48*, 9723–9731.

21. Chuang, C.-H.; Doane, T. L.; Lo, S. S.; Scholes, G. D.; Burda, C. Measuring Electron and Hole Transfer in Core/Shell Nanoheterostructures. *ACS Nano* **2011**, *5*, 6016–6024.
22. Chuang, C.-H.; Lo, S. S.; Scholes, G. D.; Burda, C. Charge Separation and Recombination in CdTe/CdSe Core/Shell Nanocrystals as a Function of Shell Coverage: Probing the Onset of the Quasi Type-II Regime. *J. Phys. Chem. Lett.* **2010**, *1*, 2530–2535.
23. Deutsch, Z.; Avidan, A.; Pinkas, I.; Oron, D. Energetics and Dynamics of Exciton−Exciton Interactions in Compound Colloidal Semiconductor Quantum Dots. *Phys. Chem. Chem. Phys.* **2011**, *13*, 3210.
24. Franzl, T.; Müller, J.; Klar, T. A.; Rogach, A. L.; Feldmann, J.; Talapin, D. V.; Weller, H. CdSe:Te Nanocrystals: Band-Edge *versus* Te-Related Emission. *J. Phys. Chem. C* **2007**, *111*, 2974–2979.
25. Avidan, A.; Oron, D. Large Blue Shift of the Biexciton State in Tellurium Doped CdSe Colloidal Quantum Dots. *Nano Lett.* **2008**, *8*, 2384–2387.
26. Avidan, A.; Deutsch, Z.; Oron, D. Interactions of Bound Excitons in Doped Core/Shell Quantum Dot Heterostructures. *Phys. Rev. B* **2010**, *82*, 165332.
27. Wang, L.-W.; Zunger, A. Local-Density-Derived Semiempirical Pseudopotentials. *Phys. Rev. B* **1995**, *51*, 17398–17416.
28. Franceschetti, A.; Fu, H.; Wang, L. W.; Zunger, A. Many-Body Pseudopotential Theory of Excitons in InP and CdSe Quantum Dots. *Phys. Rev. B* **1999**, *60*, 1819–1829.
29. Sewall, S. L.; Franceschetti, A.; Cooney, R. R.; Zunger, A.; Kambhampati, P. Direct Observation of the Structure of Band-Edge Biexcitons in Colloidal Semiconductor CdSe Quantum Dots. *Phys. Rev. B* **2009**, *80*, 081310.
30. Dexter, D. L. Theory of the Optical Properties of Imperfections in Nonmetals. In *Solid State Physics: Advances in Research and Applications*; Turnbull, D., Seitz, F., Eds.; Academic Press: New York, 1958; Vol. 6, pp 358−361.
31. Shumway, J.; Franceschetti, A.; Zunger, A. Correlation *versus* Mean-Field Contributions to Excitons, Multiexcitons, and Charging Energies in Semiconductor Quantum Dots. *Phys. Rev. B* **2001**, *63*, 155316.
32. Goede, O.; Heimbrodt, W. Isoelectronic Impurity Te in $CdS_{1-x}Se_x$ Mixed Crystals. *Phys. Status Solidi (B)* **1982**, *110*, 175–182.
33. Kuskovsky, I. L.; Tian, C.; Neumark, G. F.; Spanier, J. E.; Herman, I. P.; Lin, W.-C.; Guo, S. P.; Tamargo, M. C. Optical Properties of Δ-doped ZnSe:Te Grown by Molecular Beam Epitaxy: The Role of Tellurium. *Phys. Rev. B* **2001**, *63*, 155205.
34. Gu, Y.; Kuskovsky, I. L.; Voort, M.; van der; Neumark, G. F.; Zhou, X.; Tamargo, M. C. Zn−Se−Te Multilayers with Submonolayer Quantities of Te: Type-II Quantum Structures and Isoelectronic Centers. *Phys. Rev. B* **2005**, *71*, 045340.
35. Muller, A.; Bianucci, P.; Piermarocchi, C.; Fornari, M.; Robin, I. C.; André, R.; Shih, C. K. Time-Resolved Photoluminescence Spectroscopy of Individual Te Impurity Centers in ZnSe. *Phys. Rev. B* **2006**, *73*, 081306.
36. Sewall, S. L.; Cooney, R. R.; Anderson, K. E. H.; Dias, E. A.; Sagar, D. M.; Kambhampati, P. State-Resolved Studies of Biexcitons and Surface Trapping Dynamics in Semiconductor Quantum Dots. *J. Chem. Phys.* **2008**, *129*, 084701.
37. Sewall, S. L.; Cooney, R. R.; Dias, E. A.; Tyagi, P.; Kambhampati, P. State-Resolved Observation in Real Time of the Structural Dynamics of Multiexcitons in Semiconductor Nanocrystals. *Phys. Rev. B* **2011**, *84*, 235304.
38. Kambhampati, P. Multiexcitons in Semiconductor Nanocrystals: A Platform for Optoelectronics at High Carrier Concentration. *J. Phys. Chem. Lett.* **2012**, *3*, 1182–1190.
39. Wei, S.-H.; Zhang, S. B.; Zunger, A. First-Principles Calculation of Band Offsets, Optical Bowings, and Defects in CdS, CdSe, CdTe, and Their Alloys. *J. Appl. Phys.* **2000**, *87*, 1304–1311.
40. Wang, L.; Zunger, A. Solving Schrödinger's Equation around a Desired Energy: Application to Silicon Quantum Dots. *J. Chem. Phys.* **1994**, *100*, 2394–2397.
41. Keating, P. N. Effect of Invariance Requirements on the Elastic Strain Energy of Crystals with Application to the Diamond Structure. *Phys. Rev.* **1966**, *145*, 637–645.
42. Martin, R. M. Elastic Properties of ZnS Structure Semiconductors. *Phys. Rev. B* **1970**, *1*, 4005–4011.
43. Franceschetti, A.; Zunger, A. Direct Pseudopotential Calculation of Exciton Coulomb and Exchange Energies in Semiconductor Quantum Dots. *Phys. Rev. Lett.* **1997**, *78*, 915–918.
44. Franceschetti, A.; Troparevsky, M. C. Pseudopotential Theory of Electronic Excitations in Semiconductor Nanostructures. *J. Comput. Theor. Nanosci.* **2009**, *6*, 1272–1276.
45. An, J. M.; Califano, M.; Franceschetti, A.; Zunger, A. Excited-State Relaxation in PbSe Quantum Dots. *J. Chem. Phys.* **2008**, *128*, 164720.
46. Resta, R. Thomas−Fermi Dielectric Screening in Semiconductors. *Phys. Rev. B* **1977**, *16*, 2717–2722.